

Supplementary Materials for  
CMOS electrochemical pH localizer-imager

Han Sae Jung *et al.*

Corresponding author: Donhee Ham, donhee@seas.harvard.edu; Hongkun Park, hongkun\_park@harvard.edu

*Sci. Adv.* **8**, eabm6815 (2022)  
DOI: 10.1126/sciadv.abm6815

**The PDF file includes:**

Figs. S1 to S15  
Legends for movies S1 to S5

**Other Supplementary Material for this manuscript includes the following:**

Movies S1 to S5

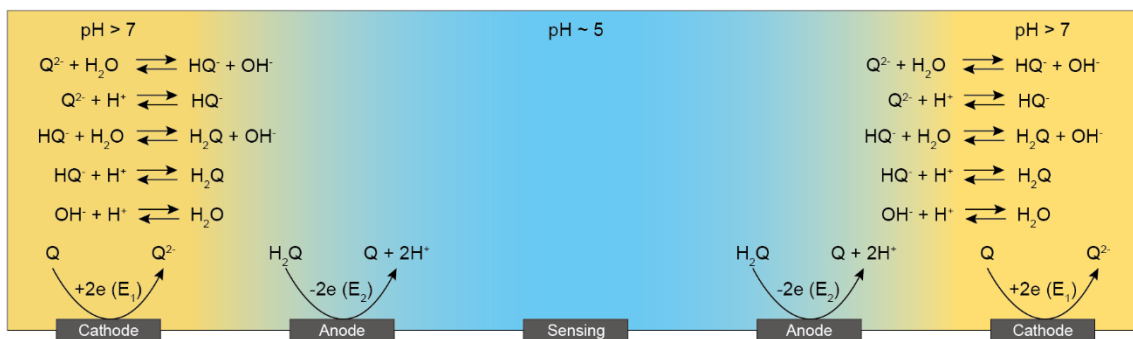


**Fig. S1 | Chemical reactions relevant to the electrochemical wall.** At the inner anodic ring, DMHQ (or H<sub>2</sub>Q) is oxidized into DMBQ (or Q), generating protons. At the outer cathodic ring, Q is reduced to a dimethyl quinone dianion (Q<sup>2-</sup>), which undergoes a series of chemical equilibria leading to generation of HQ<sup>-</sup> and OH<sup>-</sup>. The volume of base molecules, consisting of Q<sup>2-</sup>, HQ<sup>-</sup> and OH<sup>-</sup>, consumes the protons generated at the inner anodic ring not only at the cathodic ring, but also at a reasonable height from it, thus setting up the electrochemical wall that confines protons within the pixel.

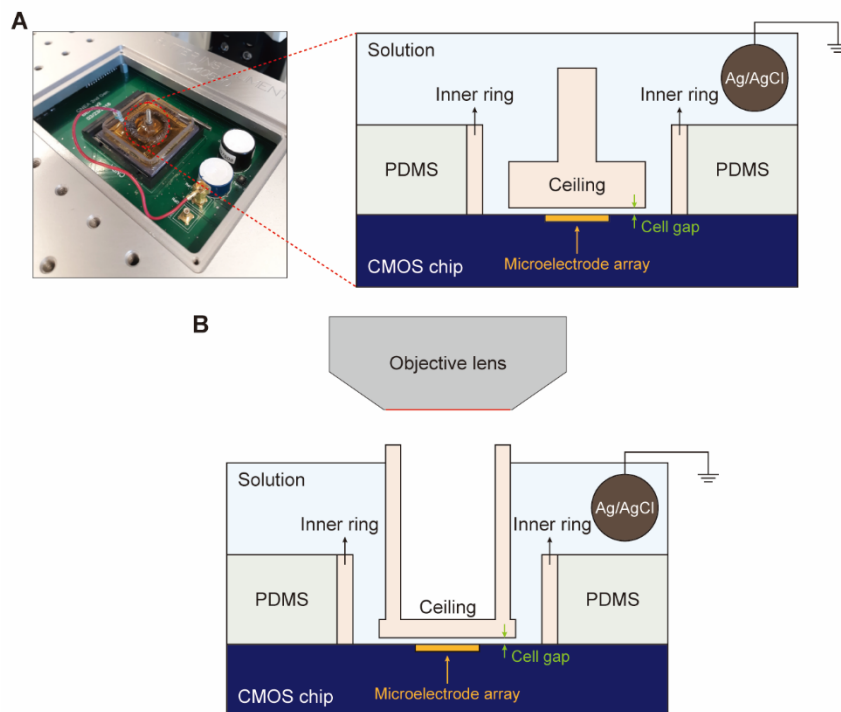


**Fig. S2 | Experimental setup.** (A) A ceiling is placed on top of the microelectrode array at a fixed height. For the ceiling spacer, photolithography was employed to create a thin SU-8 spacer layer with a thickness of about  $14\ \mu\text{m}$ . For a ceiling height of  $39\ \mu\text{m}$ , a  $25\ \mu\text{m}$  thick Kapton tape was attached to the ceiling, so that the total ceiling height becomes about  $14 + 25 = 39\ \mu\text{m}$ . The system employs an Ag/AgCl electrode as a pseudo-reference electrode, which serves as an electrical ground that counters the net current from the anodic and cathodic rings, whose currents do not in general cancel out during pH localization. So, for a positive (or negative) net current, a reduction (or an oxidation) reaction of quinones (Fig. 2A) would occur at the pseudo-reference electrode to generate a negative (or positive) counter current. (B) In the case of an epifluorescence measurement, the setup shown at the bottom is used.

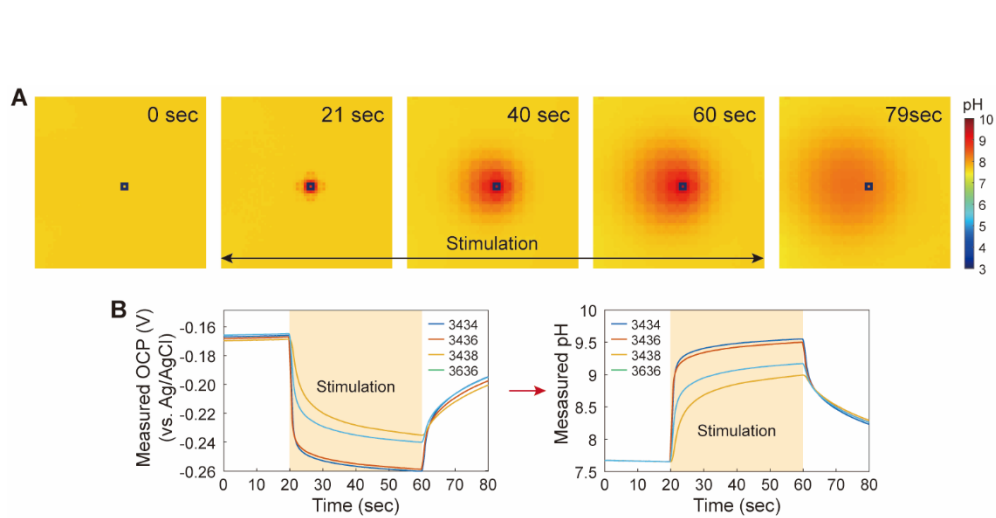


**Fig. S3 | Spatiotemporal pH imaging during a cathodic current stimulation at a single concentric ring.** (A) Spatial pH imaging over the course of current injection with  $-57$  nA. The electrochemically generated base spreads out in a radial fashion. (B) Measured OCP and pH over time. The ceiling height is about  $39 \mu\text{m}$ .

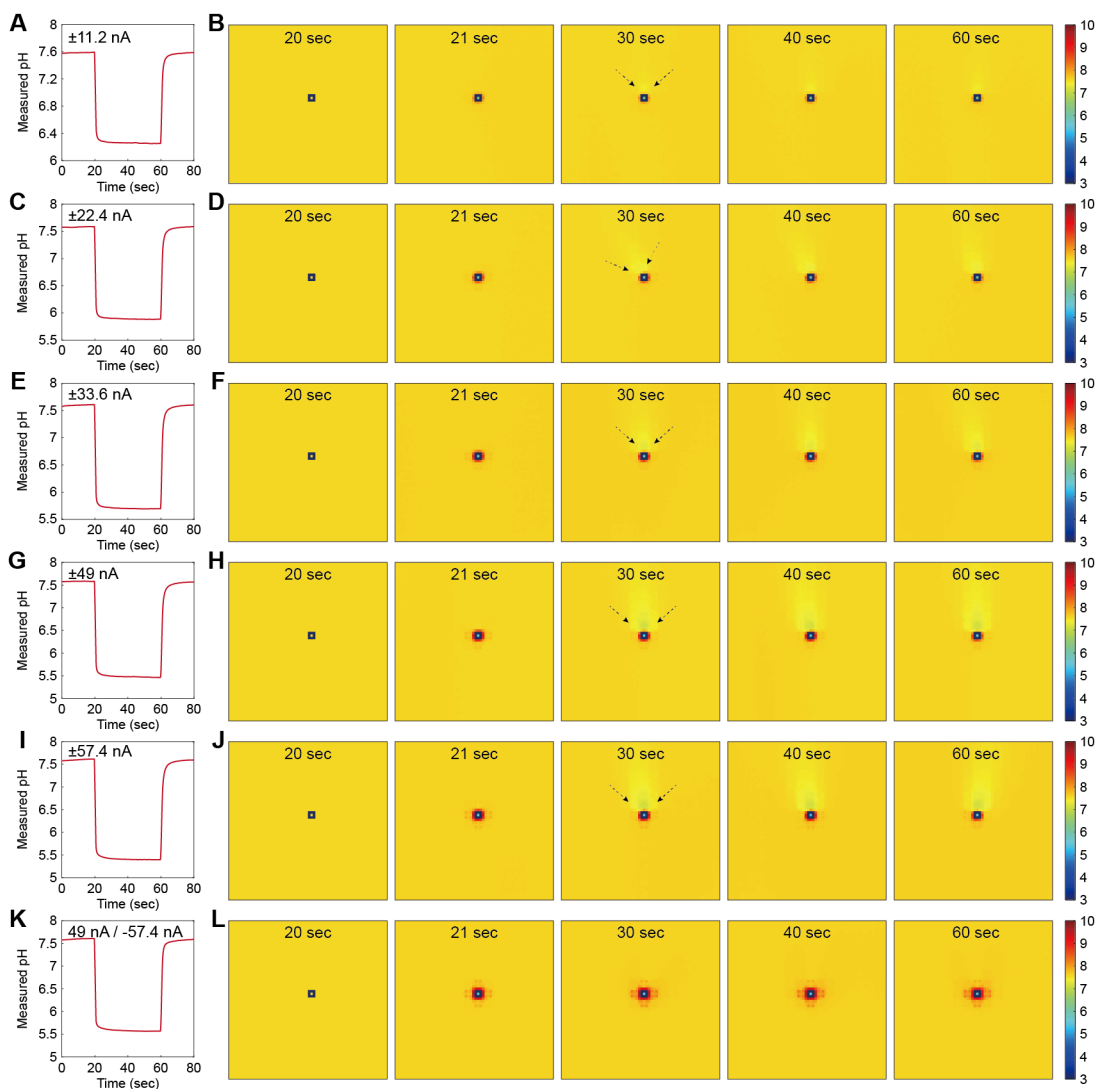


**Fig. S4 | Current stimulation with unequal or equal magnitudes of anodic and cathodic currents.** (A-B) Spatiotemporal pH monitoring during current injection with 11 nA and -9 nA. (C-D) Spatiotemporal pH monitoring during current injection with 22 nA and -19 nA. (E-F) Spatiotemporal pH monitoring during current injection with 33 nA and -28 nA. (G-H) Spatiotemporal pH monitoring during current injection with 48 nA and -41 nA. (I-J) Spatiotemporal pH monitoring during current injection with 56 nA and -48 nA. (K-L) Spatiotemporal pH monitoring during current injection with  $\pm 48$  nA. In all cases, no ceiling was placed on top of the electrode array. Also, in all cases, the solution composition was 10 mM DMHQ, 5 mM DMBQ, 1 M NaCl (aq), 1.9 M NaNO<sub>2</sub> (aq), and 5% v/v DMSO.

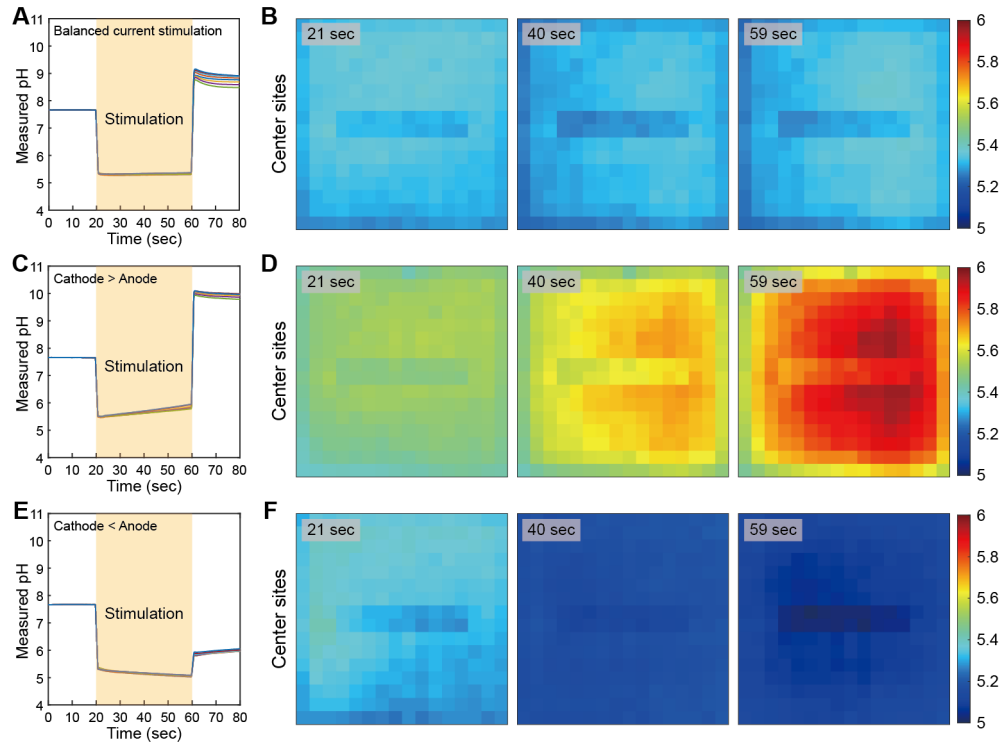


**Fig. S5 | Electrochemical pH localization with optimal and non-optimal balance of anodic and cathodic currents.** (A) Localized pH values measured at the pixel center OCP sensors during stimulation of all 256 pixels with  $\pm 48$  nA. The anodic and cathodic currents are optimally balanced, resulting in a stable pH value over time. (B) pH maps during stimulation of all 256 pixels with  $\pm 48$  nA. (C) Localized pH values measured at the pixel center OCP sensors during stimulation of all 256 pixels with 47 nA of anodic current and -48 nA of cathodic current. The cathodic current overwhelms the anodic current, resulting in pH values rising over time. (D) pH maps during stimulation of all 256 pixels with 47 nA of anodic current and -48 nA of cathodic current. The cathodic current overwhelms the anodic current, resulting in pH values rising over time (the colors become redder). (E) Localized pH values measured at the pixel center OCP sensors during stimulation of all 256 pixels with 49 nA of anodic current and -48 nA of cathodic current. The anodic current overwhelms the cathodic current, resulting in pH values dropping over time. (F) pH maps during stimulation of all 256 pixels with 49 nA of anodic current and -48 nA of cathodic current. The anodic current overwhelms the cathodic current, resulting in pH values dropping over time (the colors become bluer). The ceiling height is about 39  $\mu\text{m}$  for all cases.

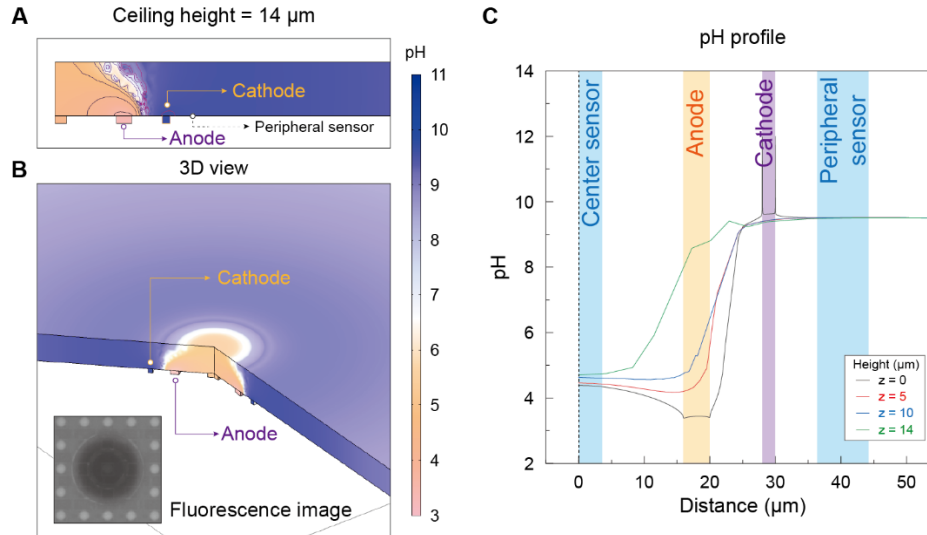


**Fig. S6 | COMSOL simulation of pH localization with 14 μm ceiling height with an anodic current of 76 nA and a cathodic current of -76 nA. (A) Cross-sectional pH distribution. Purple lines: pH contours. (B) 3D pH distribution. (C) pH vs. lateral distance from cell center at various  $z$  (vertical distance from the chip surface) positions. Acidic pH ( $\text{pH} < 7$ ) localization clearly manifests in all three parts of the figure. The localized acidic pH region extends all the way to the ceiling, with its cross-sectional area shrinking with increasing  $z$ . For example, in part C: at  $z = 0$  (chip surface), the acidic pH region extends to what is between anode and cathode; at  $z = 14 \mu\text{m}$  (ceiling), the acidic pH region shrinks to inside the anodic ring; and at the cell center, strong acidity ( $\text{pH} < 5$ ) is maintained along  $z$ . The pH map presented in three different ways here is the steady-state  $[\text{H}^+]$  diffusion profile. The localized acidic pH region ( $\text{pH} < 7$ , or  $[\text{H}^+] > [\text{base}]$ )—which is well within the cathodic ring—is surrounded by the basic pH environment ( $\text{pH} > 7$ , or  $[\text{H}^+] < [\text{base}]$ ), with a very steep pH gradient in lateral directions, *i.e.*, with  $[\text{H}^+]$  concentration changing by several orders of magnitude over the lateral distance of tens of μm.**

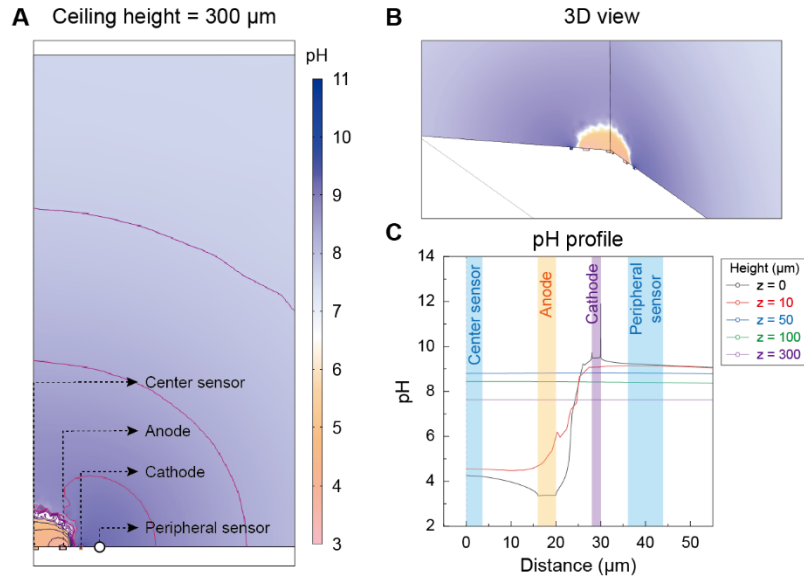


**Fig. S7 | COMSOL simulation of pH localization with 300  $\mu\text{m}$  ceiling height with an anodic current of 73 nA and a cathodic current of -73 nA. (A) Cross-sectional pH distribution. Purple lines: pH contours. (B) 3D pH distribution. (C) pH vs. lateral distance from cell center at various  $z$  positions. All three parts of the figure again clearly show acidic pH ( $\text{pH} < 7$ ) localization now with a ceiling 300  $\mu\text{m}$  above, which practically models a situation with no ceiling. In this case, the localized acidic pH region does not extend all the way to the ceiling, but is confined within a hemisphere, with the basic wall now formed not just on the sides of, but also above, the acidic pH region. Again, the acidic pH region narrows as  $z$  increases. At the cell center well within the hemisphere, strong acidity ( $\text{pH} < 5$ ) is maintained along  $z$ .**

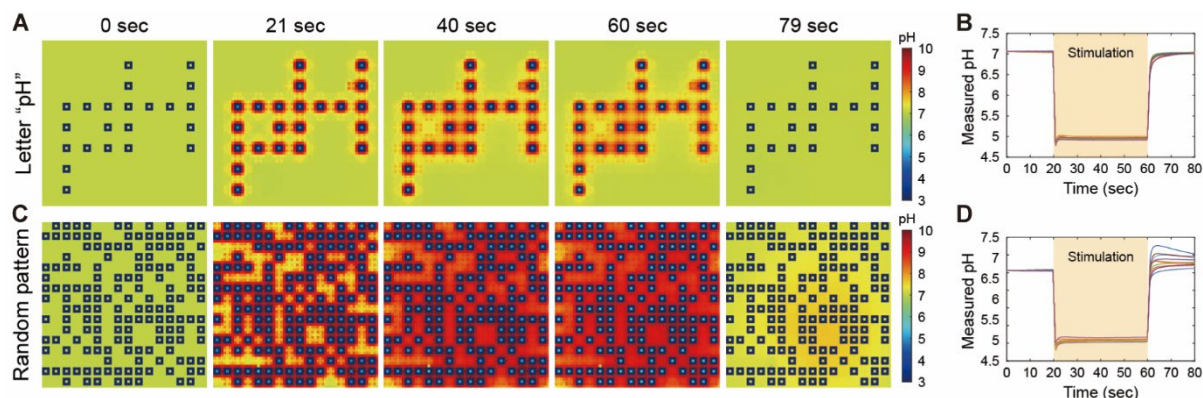


**Fig. S8 | Electrochemical pH localization with additional stimulation patterns.** (A-B), pH localization with a letter “pH”. Median/standard deviation at  $t = 40$  s is 4.94/0.02. (C-D), pH localization with a random pattern. Note that this random pattern is different from the selected pattern shown in Fig. 3C. Median/standard deviation at  $t = 40$  s is 5.06/0.05. The applied anodic and cathodic currents are 62 nA and -62 nA. Here, the solution contains 10 mM DMHQ, 5 mM DMBQ, 1 M NaCl, 0.7 M NaNO<sub>2</sub>, and 5% v/v DMSO. The ceiling height is about 50  $\mu$ m.

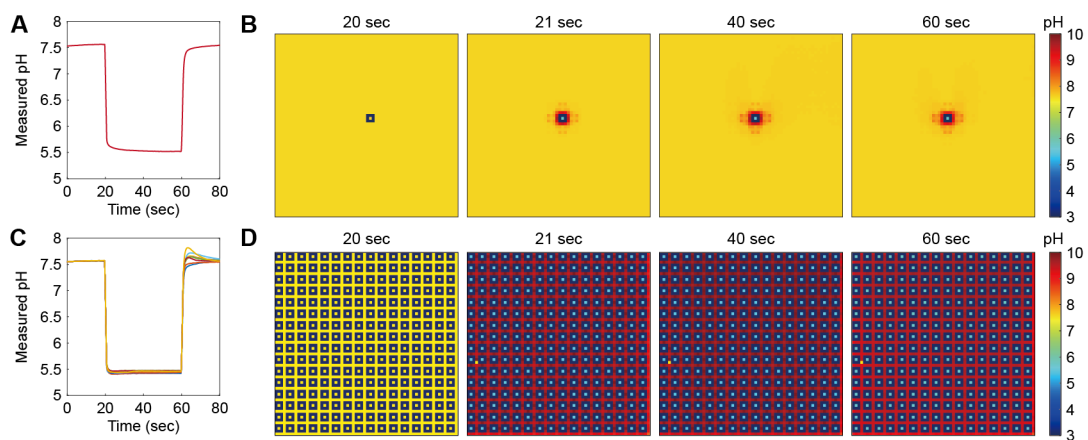


**Fig. S9 | Electrochemical pH localization with no ceiling.** (A) Localized pH value measured at the pixel center OCP sensor during stimulation of a single pixel with  $\pm 48$  nA. (B) pH maps during stimulation of a single pixel with  $\pm 48$  nA. (C) Localized pH values measured at the pixel center OCP sensors during stimulation of all 256 pixels with  $\pm 48$  nA. (D) pH maps during stimulation of all 256 pixels with  $\pm 48$  nA. In all cases, no ceiling was placed on top of the electrode array. Also, in all cases, the solution composition was 10 mM DMHQ, 5 mM DMBQ, 1 M NaCl (aq), 1.9 M  $\text{NaNO}_2$  (aq), and 5% v/v DMSO.

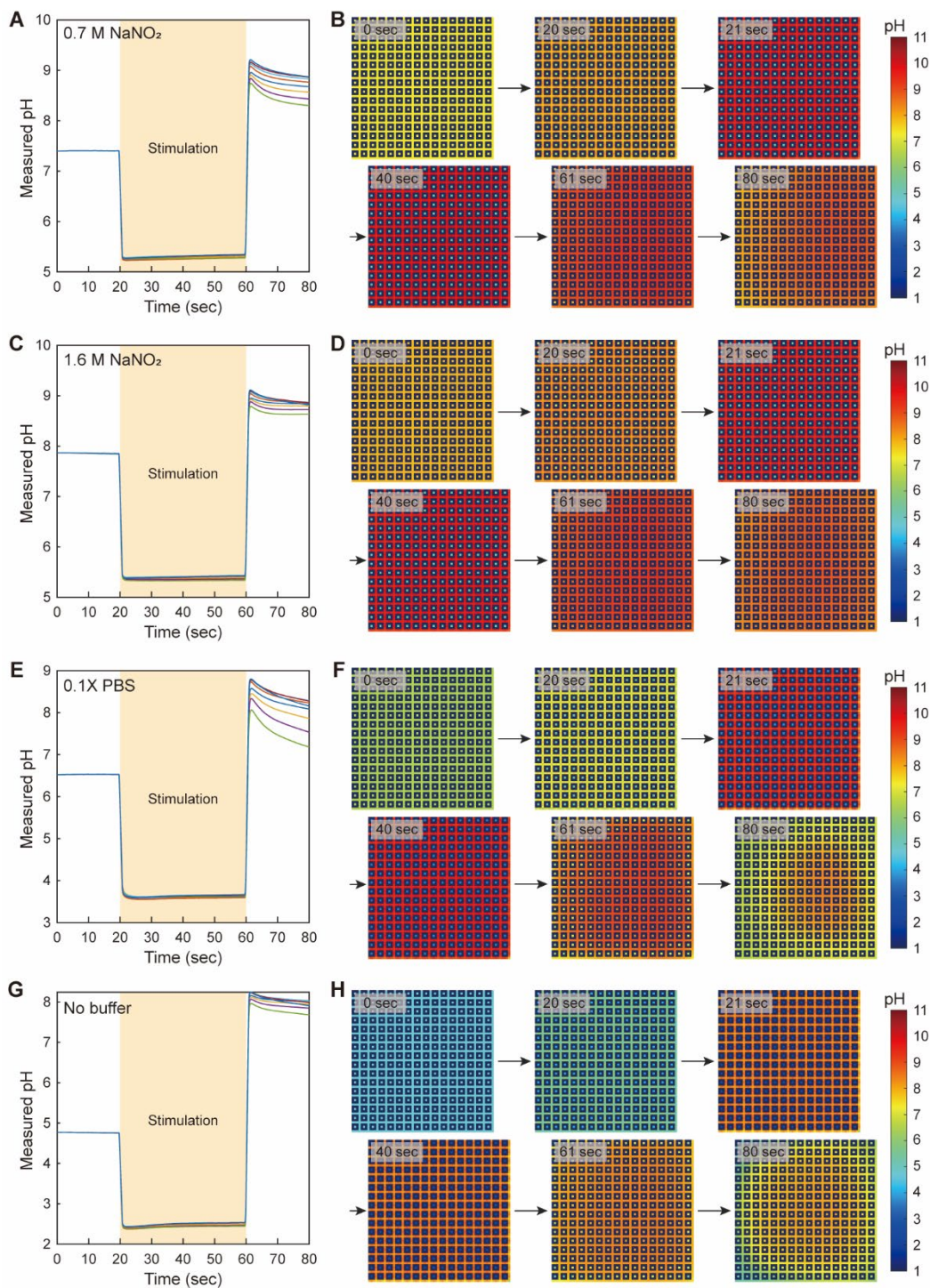


**Fig. S10 | Electrochemical pH localization with various solution compositions.** (A-B) pH localization result with 0.7 M NaNO<sub>2</sub> (aq). (C-D) pH localization result with 1.6 M NaNO<sub>2</sub> (aq). (E-F) pH localization result with 0.1 X phosphate-buffered saline (PBS) solution. (G-H) pH localization result with no pH buffer. All solutions also contain 10 mM DMHQ, 5 mM DMBQ, 1 M NaCl, and 5% v/v DMSO. For all solutions, 48 nA of anodic current and -48 nA of cathodic current were applied during the stimulation period.

current were applied for 40 seconds. pH was successfully localized in all cases, regardless of the solution composition. The ceiling height is about 39  $\mu\text{m}$  for all cases.

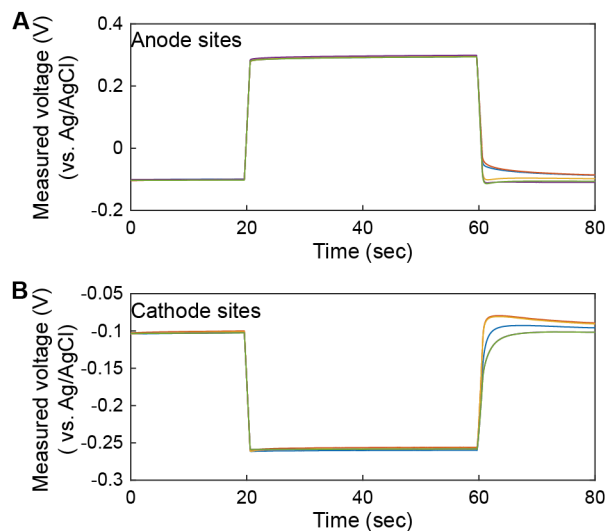


**Fig. S11 | Measured voltages at the anodes and cathodes during current injection. (A)** Measured voltages at an exemplary subset of anodes during current injection with  $\pm 57$  nA at randomly selected pixels from the experiment shown in Fig. 3D. **(B)** Measured voltages at an exemplary subset of cathodes during current injection with  $\pm 57$  nA of cathodic current at randomly selected pixels from the experiment shown in Fig. 3D.

The measured stimulation voltages at the randomly selected sites were around 0.3 V and -0.25 V at the anodes and cathodes, respectively, indicating that when injecting a balanced current ratio, the oxidation and reduction reactions occurred as desired. Moreover, these voltages remained constant throughout the stimulation, indicating that the injected currents were Faradaic in nature (except at the very start and end of the stimulation), because a capacitive current requires a changing stimulation voltage. Note that there may be some perturbations during the transitions with non-Faradaic currents, but these perturbations are transient that quickly settle: that is why in the region with constant Faradaic currents, the measured anodic and cathodic voltages and the measured OCP remain constant. The Faradaic nature of the injected currents implies that the rates of the redox reactions were being directly controlled, a key requirement for achieving an optimal balance of acid and base generations such that an acidic pH is stably localized.

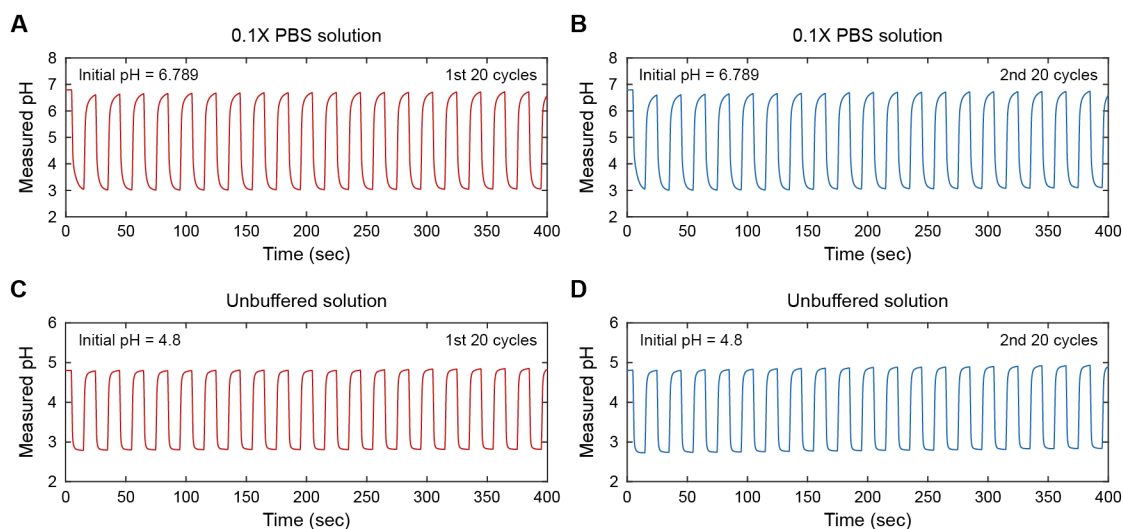


**Fig. S12 | Localized pH during application of two sets of 20 current pulses in different solution compositions. (A-B) Localized pH over time in a 0.1 X PBS solution for the first set of 20 pulses and the second set of 20 pulses. (C-D) Localized pH over time in an unbuffered solution for the first set of 20 pulses and the second set of 20 pulses. The localized pH value was consistent between the two sets for both solution compositions. In all cases, 10 mM DMHQ, 5 mM DMBQ, 1 M NaCl (aq), and 5% v/v DMSO were used with no ceiling.**

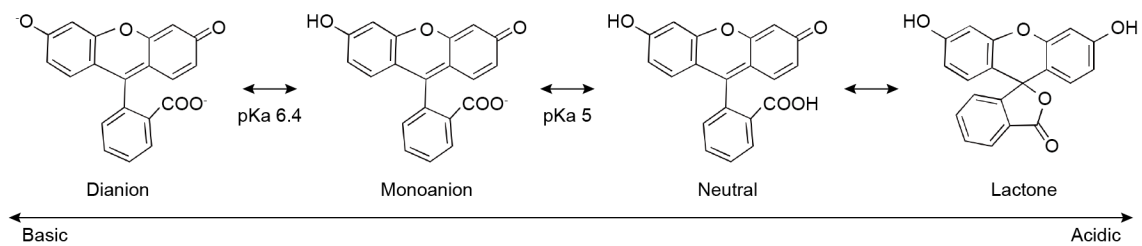


**Fig. S13 | pH-dependent chemical equilibria of fluorescein.** Fluorescein is fluorescent in only its dianionic or monoanionic form. Once it's fully protonated and becomes neutral, it is no longer fluorescent.

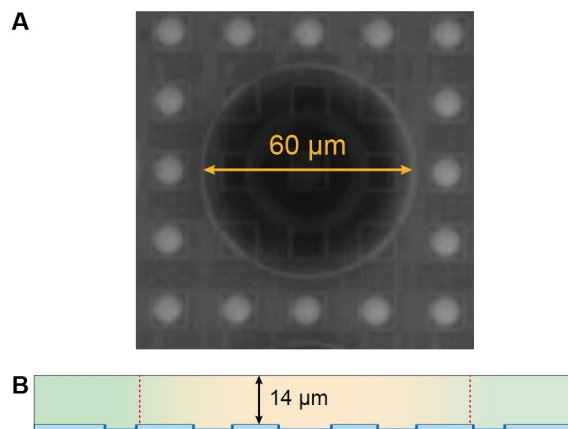


**Fig. S14 | Volume of the localized aqueous acid.** (A) An epifluorescence image during localization of acidic pH. Inside the cathode (diameter = 60  $\mu\text{m}$ ), the pH-dependent fluorescence intensity decreased locally, as a result of localizing pH  $\sim 5.54$ . (B) By approximating the localized volume as a cylinder, the volume of the localized aqueous acid (inside of cathode ring) is estimated to be about  $\pi \times (30 \mu\text{m})^2 \times 14 \mu\text{m} \times 10^{-3} \text{ pL} / \mu\text{m}^3 = 40 \text{ pL}$ .

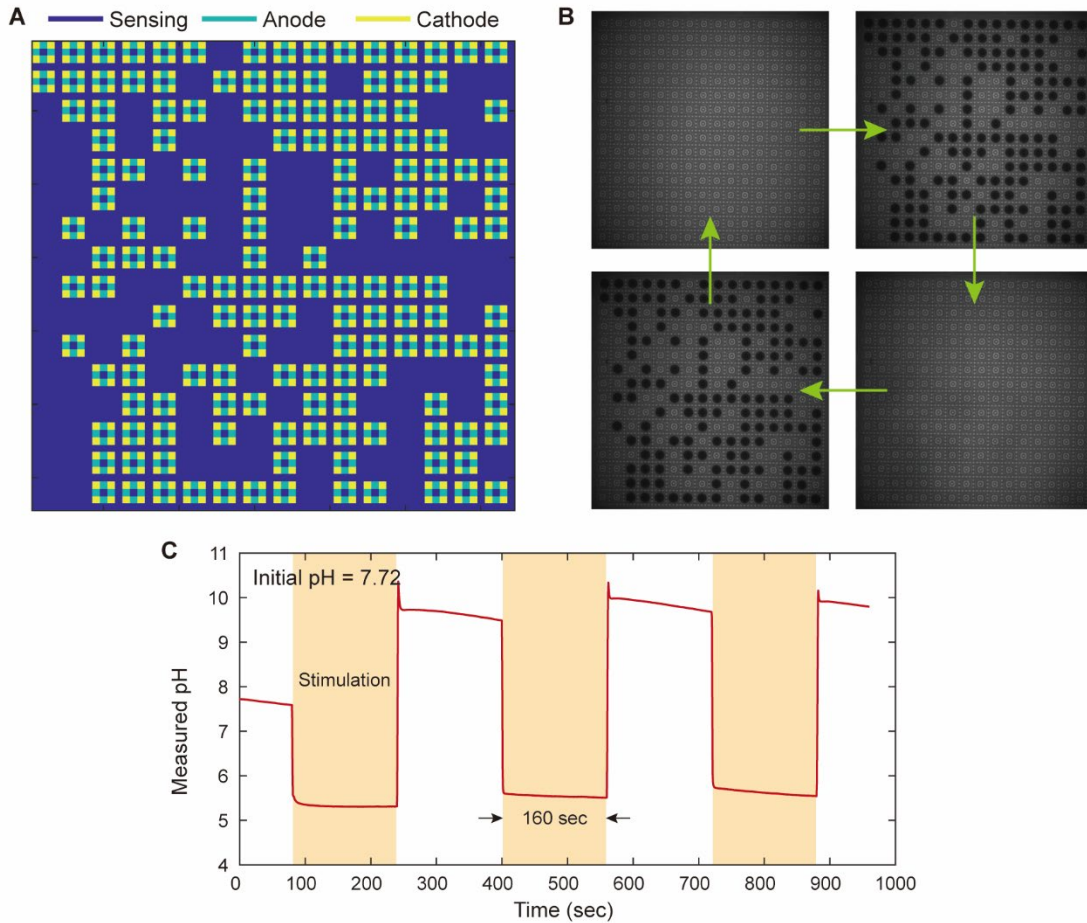


**Fig. S15 | Concurrent monitoring of pH with pixel center OCP sensors and epifluorescence microscopy during a current pulse stimulation. (A)** Schematic of the stimulation pattern. **(B)** Epifluorescence pH monitoring during a current pulse stimulation. **(C)** pH measured over time. Three current pulses were applied with 160-s pulse duration and 160-s time lapse. For each pulse, 48 nA of anodic current and -48 nA of cathodic current were applied. The ceiling height is about 14  $\mu\text{m}$ .

**Movie S1 | Spatiotemporal imaging of pH diffusion during current stimulation at a single concentric ring.** (Left) a real-time imaging of acidic pH diffusion when only the anodic ring is activated with a 57 nA current injection. (Right) a real-time imaging of basic pH diffusion when only the cathodic ring is activated with a -57 nA current injection.

**Movie S2 | Array-wide pH localization for various stimulation patterns.** Spatiotemporal pH profiles during current stimulation of a single pixel (left), all 256 pixels (middle), and randomly selected pixels (right), with each activated pixel injecting an anodic current of 57 nA and a cathodic current of -57 nA. The left, middle, and right movies correspond to the experiments of Fig. 3A, Fig. 3D top, and Fig. 3D bottom, respectively.

**Movie S3 | Success and failure of array-wide pH localization with optimal and non-optimal balance of anodic and cathodic currents.** This is the real-time movie of fig. S5. Successful pH localization in all pixels is obtained with each pixel injecting an anodic current of 48 nA and a cathodic current of -48 nA with the optimal ratio of 1:-1 (movie on the left; this corresponds to fig. S5B). On the other hand, acidic pH breaks out and pH localization fails, if each pixel injects an anodic current of 49 nA and a cathodic current of -48 nA (movie on the right; this corresponds to fig. S5F).

**Movie S4 | Comparison of pH localization capability to an electrode array with a different pixel structure.** Top two videos (identical to the left and middle of movie S2) show pH localization experiments with our concentric pixel and its array. One solely activated pixel achieves a pH localization with an anodic current of 57 nA and a cathodic current of -57 nA (top, left). When these pixel currents  $\pm 57$  nA are applied to all pixels, pH localization is obtained at all pixels (top, right). That is, the pixel currents optimal for a single pixel activation remains optimal for all-pixel activation, demonstrating no crosstalk between activated pixels. Bottom two videos show pH localization experiments with a discontinuous anode/cathode pixel and its  $10 \times 10$  array. The discontinuous anode/cathode pixel consists of an OCP sensor at its center, 8 surrounding anodes, and 16 surrounding cathodes. In this pixel, all electrodes are Pt circle electrodes with 8  $\mu\text{m}$  diameter. In its arrayed arrangement, we implement peripheral OCP sensors as we did in the concentric pixel array. One solely activated pixel achieves a pH localization with an anodic current of 94 nA and a cathodic current of -284 nA (bottom, left). When these currents of 94 nA and -284 nA are applied to all pixels, pH localization fails, *i.e.*, acids break out (bottom, right). So in this case, the pixel currents optimal for a single pixel activation are not optimal for all-pixel activation, due to crosstalk between activated pixels.

**Movie S5 | Concurrent monitoring of pH with pixel center OCP sensors and an epifluorescence microscope during a current pulse stimulation.** The spatiotemporal pH profiles monitored by pixel center OCP sensors and an epifluorescence microscope were consistent throughout a current pulse stimulation with 5-s pulse duration and 5-s time lapse, thus confirming accurate encoding of pH-gated molecular states at the selected sites. For each pulse, each activated pixel had a 48 nA of anodic current and a -48 nA of cathodic current. The ceiling height is about 14  $\mu\text{m}$ .